Journal of Solid Mechanics Vol. 3, No. 4 (2011) pp. 379-391

Electro-Mechanical Buckling of a Piezoelectric Annular Plate Reinforced with BNNTs Under Thermal Environment

A. Ghorbanpour Arani[1,2,*], E. Haghparast[1]

[1] *Faculty of Mechanical Engineering, University of Kashan, Kashan, Islamic Republic of Iran*
[2] *Institute of Nanoscience & Nanotechnology, University of Kashan, Kashan, Islamic Republic of Iran*

Received 7 November 2011; accepted 15 December 2011

ABSTRACT

In this article, axisymmetric buckling behavior of piezoelectric fiber reinforced polymeric composite (PFRPC) annular plate subjected to electro-thermo-mechanical field is presented utilizing principle of minimum potential energy. Boron-nitride nanotubes (BNNTs) are used as fibers. Full coupling between electrical, mechanical and thermal fields are considered according to a representative volume element (RVE)-based XY piezoelectric fiber reinforce composite (PEFRC) model. Assuming PFRPC material and its composite constituents to be linear, homogenous, orthotropic, and perfectly bonded with uniform applied field, the basic relation for the axisymmetric buckling of a circular plate subjected to radial compression, radial electrical field, and uniform temperature change ΔT are derived. The presented results show that BNNTs can be used as an effective supplement to improve mechanical behavior of polyvinylidene fluoride (PVDF). Also, at normal working conditions, the influence of thermal and mechanical fields is much higher than the electric one on the critical load; hence, this smart structure is best suited for applications as sensors than actuators.

Keywords: Axisymmetric buckling; BNNT; Annular plate; Piezoelectric polymeric; Energy method; Electro-thermo-mechanical loadings

1 INTRODUCTION

BNNTs, discovered in the mid 1990s [1-2], in addition to carbon nanotubes (CNTs) properties like high chemical stability and superior mechanical properties have oxidation resistance at higher temperatures, high thermal conductivity and piezoelectricity [3-4]. In comparison with metallic or semiconducting CNTs, a BNNTs are an electrical insulator with a band gap of ca. 5 eV, and therefore independent of tube geometry; hence it is more suitable for composite reinforcement than CNTs [5]. In 1969, Kawai discovered a significant piezoelectric effect in PVDF and in conjunction with excellent mechanical properties and continuous application of temperature, PVDF has since been studied extensively [6-7].

Composites of BNNTs dispersed in ceramic or polymeric matrices have attracted a considerable attention in recent years due to their potential applications in aeronautic and astronautic technology, automobile, electronic and mechanical devices, power generation, sensors, actuators, ultrasonic transducers, chemical vessels and many other modern industries [8-10]. Najafizadeh and Heydari [11] investigated mechanical buckling of circular plates composed of functionally graded materials (FGMs) based on higher order deformation plate theory (HSDT). Their study shows that HSDT accurately predicts the behavior of functionally graded circular plate. Ghorbanpour Arani et

* Corresponding author. Tel.: +98 9131626594 ; Fax: +98 361 55912424.
E-mail address: aghorban@kashanu.ac.ir (A.Ghorbanpour Arani).

al. [12] investigated the buckling analysis of laminated composite plates reinforced by single-walled carbon nanotubes (SWCNTs) using an analytical approach as well as the finite element method. Their developed model is based on the classical laminated plate theory (CLPT) and the third-order shear deformation theory (TSDT) for moderately thick laminated plates. Elastic buckling of circular annular plate reinforced with carbon nanotubes under compressive and torsional loads are studied by Jam et al. [13]. Their model is based on the CLPT. They used Mori-Tanaka method to evaluate the effective elastic properties of nanocomposite. The influence of CNTs orientation, boundary conditions and geometric ratio of plate and agglomeration of the randomly oriented straight CNTs are investigated on the critical buckling loads.

Vodenitcharova and Zhang [14] studied the pure bending and bending-induced local buckling of a nanocomposite beam reinforced by a SWCNT. They found that in thicker matrix layers the SWNT buckles locally at smaller bending angles and greater flattening ratios. Shen and Zhang [15] studied thermal post-buckling behavior of functionally graded carbon nanotube-reinforced composite plates subjected to in-plane temperature variation based on a micromechanical model and multi-scale approach. Their results indicated that the thermal post-buckling behaviors of CNT reinforced composite plates were significantly influenced by the thermal load ratio, the transverse shear deformation, the plate aspect ratio as well as the CNT volume fraction. Baltaci et al. [16] investigated the behavior of buckling of laminated composite circular plates having circular holes and subjected to uniform radial load using finite element method. They consider the effects of whole sizes, location of the holes, thickness variations and boundary conditions on buckling load. Seifi et al. [17] investigated buckling of composite annular plates under uniform internal and external radial edge loads using energy method. They consider symmetric cross-ply laminates and study the influence of some parameters like thickness, stacking sequence, type of supports and the ratio of hole to sheet radius on load of buckling.

Motivated by these considerations, this work aims to study the electro-thermo-mechanical axisymmetric buckling of piezoelectric polymeric circular plate reinforced with BNNTs. The present paper develops the principle of minimum total potential energy to obtain the critical buckling load. Simply supported and clamped boundary conditions are considered. Applying uniform electrical and thermal fields to a layer of PVDF circular plate reinforced by BNNTs, this work attempts to verify the influence of thermal and electrical fields on buckling strength of circular plate composites.

2 MICRO-MECHANIC MODEL

As mentioned above, the overall properties of the PEFRC is evaluated by a micro-mechanic XY model [18]. A representative volume element (RVE) with square cross-sectional is selected for a PEFRC and a circular one for the fiber is assumed [18]. The influence of the piezoelectric fiber volume fraction on the effective constants for PEFRC materials using the above mentioned model was investigated and the results complied fairly well with those found with Mori-Tanaka mean field approach. The assumptions made for the XY model include:

(i) The composite material is perfectly bonded, its constituents are assumed to be linear homogeneous and orthotropic.
(ii) The applied electric and thermal fields to the PEFRC unit cell are uniform.
(iii) Iso-stress, iso-electric displacement, are assumed to exist across the planes which are in series with respect to the loading direction. Iso-strain and iso-electric field are assumed across the planes which are in parallel with respect to the loading direction [6].
(iv) Thermal field within a PEFRC unit cell is uniform.

The closed-form formulas for the effective electro-thermo-elastic constants of an X PEFRC strip may be expressed as Eqs. (1) to (11) described below [18] :

$$C^{p}_{11} = \frac{C^{mm}_{11}\, C^{pp}_{11}}{\rho C^{mm}_{11} + (1-\rho) C^{pp}_{11}} \tag{1}$$

$$C^{p}_{22} = \rho C^{pp}_{22} + (1-\rho) C^{mm}_{22} + \frac{(C^{p}_{12})^2}{(C^{p}_{11})} - \rho \frac{(C^{pp}_{12})^2}{C^{pp}_{11}} - \frac{(1-\rho)(C^{mm}_{12})^2}{C^{mm}_{11}} \tag{2}$$

$$C_{23}^{p} = \rho C_{23}^{pp} + (1-\rho)C_{23}^{mm} + \frac{C_{12}^{p}C_{13}^{p}}{C_{11}^{p}} - \rho\frac{C_{12}^{pp}C_{13}^{pp}}{C_{11}^{pp}} - \frac{(1-\rho)C_{12}^{mm}C_{13}^{mm}}{C_{11}^{mm}} \tag{3}$$

$$C_{13}^{p} = C_{11}^{p}\left[\frac{\rho C_{13}^{pp}}{C_{11}^{pp}} - \frac{(1-\rho)C_{13}^{mm}}{C_{11}^{mm}}\right] \tag{4}$$

$$C^{p}{}_{33} = \rho C_{33}^{pp} + (1-\rho)C_{33}^{mm} + \frac{(C_{13}^{p})^2}{C^{p}{}_{12}} - \rho\frac{(C_{3}^{pp})^2}{C_{11}^{pp}} - \frac{(1-\rho)(C_{13}^{mm})^2}{C_{11}^{mm}} \tag{5}$$

$$e^{p}{}_{31} = C_{11}^{p}\left[\frac{\rho e_{13}^{pp}}{C_{11}^{pp}} - \frac{(1-\rho)e_{13}^{mm}}{C_{11}^{mm}}\right] \tag{6}$$

$$e^{p}{}_{32} = \rho e_{23}^{pp} + (1-\rho)e_{23}^{mm} + \frac{C_{12}^{p}e_{13}^{p}}{C_{11}^{p}} - \rho\frac{C_{12}^{pp}e_{13}^{pp}}{C_{11}^{pp}} - \frac{(1-\rho)C_{12}^{mm}e_{13}^{mm}}{C_{11}^{mm}} \tag{7}$$

$$e^{p}{}_{33} = \rho e_{33}^{pp} + (1-\rho)e_{33}^{mm} + \frac{C_{13}^{p}e_{13}^{p}}{C_{11}^{p}} - \rho\frac{C_{13}^{pp}e_{13}^{pp}}{C_{11}^{pp}} - \frac{(1-\rho)C_{13}^{mm}e_{13}^{mm}}{C_{11}^{mm}} \tag{8}$$

$$\lambda_{1}^{p} = C_{11}^{p}\left[\frac{\rho\lambda_{1}^{pp}}{C_{11}^{pp}} - \frac{(1-\rho)\lambda_{11}^{mm}}{C_{11}^{mm}}\right] \tag{9}$$

$$\lambda_{3}^{p} = \rho\lambda_{3}^{pp} + (1-\rho)\lambda_{3}^{mm} + \frac{C_{13}^{p}\lambda_{1}^{p}}{C_{11}^{p}} - \rho\frac{C_{13}^{pp}\lambda_{2}^{p}}{C_{11}^{pp}} - \frac{(1-\rho)C_{13}^{mm}\lambda_{1}^{mm}}{C_{11}^{mm}} \tag{10}$$

$$\lambda_{2}^{p} = \rho\lambda_{22}^{pp} + (1-\rho)\lambda_{22}^{mm} + \frac{C_{12}^{p}\lambda_{1}^{p}}{C_{11}^{p}} - \rho\frac{C_{12}^{pp}\lambda_{2}^{p}}{C_{11}^{pp}} - \frac{(1-\rho)C_{12}^{mm}\lambda_{1}^{mm}}{C_{11}^{mm}} \tag{11}$$

where C_{ij}, e_{mn} and λ_{p}, are elastic stiffness constants, piezoelectric constants and thermal expansion, respectively. The constant ρ is $x_a / x_b = y_a / y_b$ where x_a, x_b and y_a, y_b are dimensions of fiber and matrix unit cells, respectively as illustrated in Fig. 1. For the Y PEFRC model, the corresponding equations can be obtained by simply exchanging the subscripts 1 with 2 in the above Eqs. (1.1-1.10). Hence, the effective constants of XY model was obtained by placing the effective constitutive coefficients of X model into the effective fiber coefficients of Y model. The resulting formulations are presented in Eqs. (12- 23) below which represent the mechanical properties for the defined RVE

$$C_{11} = \rho C_{11}^{p} + (1-\rho)C_{11}^{m} + \frac{C_{12}^{2}}{C_{22}} - \rho\frac{(C_{12}^{p})^2}{C_{22}^{p}} - \frac{(1-\rho)(C_{12}^{m})^2}{C_{22}^{m}} \tag{12}$$

$$C_{12} = C_{22}\left[\frac{\rho C_{12}^{p}}{C_{22}^{p}} - \frac{(1-\rho)C_{12}^{m}}{C_{22}^{m}}\right] \tag{13}$$

$$C_{13} = \rho C_{13}^{p} + (1-\rho)C_{13}^{m} + \frac{C_{12}C_{23}}{C_{22}} - \rho\frac{C_{12}^{p}C_{23}^{p}}{C_{22}^{p}} - \frac{(1-\rho)C_{12}^{m}C_{23}^{m}}{C_{22}^{m}} \tag{14}$$

$$C_{22} = \frac{C_{22}^{p}C_{22}^{m}}{\rho C_{22}^{m} + (1-\rho)C_{22}^{p}} \tag{15}$$

$$C_{23} = C_{22}\left[\frac{\rho C_{23}^{2}}{C_{22}^{p}} - \frac{(1-\rho)C_{23}^{m}}{C_{22}^{m}}\right] \tag{16}$$

$$C_{33} = \rho C_{33}^{p} + (1-\rho)C_{33}^{m} + \frac{C_{23}^{2}}{C_{22}} - \rho\frac{(C_{23}^{p})^2}{C_{22}^{p}} - \frac{(1-\rho)(C_{23}^{m})^2}{C_{22}^{m}} \tag{17}$$

$$e_{31} = \rho e_{31}^{p} + (1-\rho)e_{31}^{m} + \frac{C_{12}e_{32}}{C_{22}} - \rho\frac{C_{12}^{p}e_{32}^{p}}{C_{22}^{p}} - \frac{(1-\rho)C_{12}^{m}e_{32}^{m}}{C_{22}^{m}} \tag{18}$$

$$e_{32} = C_{22}\left[\frac{\rho e_{32}^{2}}{C_{22}^{p}} - \frac{(1-\rho)e_{32}^{m}}{C_{22}^{m}}\right] \tag{19}$$

$$e_{33} = \rho e_{33}^{p} + (1-\rho)e_{33}^{m} + \frac{C_{23}e_{32}}{C_{22}} - \rho\frac{C_{23}^{p}e_{32}^{p}}{C_{22}^{p}} - \frac{(1-\rho)C_{23}^{m}e_{32}^{m}}{C_{22}^{m}} \tag{20}$$

$$\lambda_1 = \rho\lambda_1^{p} + (1-\rho)\lambda_1^{m} + \frac{C_{12}\lambda_2}{C_{22}} - \rho\frac{C_{12}^{p}\lambda_2^{p}}{C_{22}^{p}} - \frac{(1-\rho)C_{12}^{m}\lambda_2^{m}}{C_{22}^{m}} \tag{21}$$

$$\lambda_3 = \rho\lambda_3^{p} + (1-\rho)\lambda_3^{m} + \frac{C_{23}\lambda_2}{C_{22}} - \rho\frac{C_{23}^{p}\lambda_2^{p}}{C_{22}^{p}} - \frac{(1-\rho)C_{23}^{m}\lambda_2^{m}}{C_{22}^{m}} \tag{22}$$

$$\lambda_2 = C_{22}\left[\frac{\rho\lambda_2^{p}}{C_{22}^{p}} - \frac{(1-\rho)\lambda_2^{m}}{C_{22}^{m}}\right] \tag{23}$$

3 FORMULATION

3.1 Properties of piezoelectric polymeric composites

Effective properties of PFRPC with square piezoelectric fiber and unit cell cross-sections were obtained using approach adopted by Tan and Tong [18] in which they use RVE model. The closed-form formulas are derived using linear piezoelectric theory and iso-field assumptions under multiple loads including iso-strain, iso-stress, iso-electric field, and iso-electric displacement.

3.2 Electro-mechanical coupling

Considering the fact that electro-mechanical behavior of the material is elastic and linear, the coupling between the corresponding mechanical and electrostatic fields will be limited to the linear case and is assumed as such. Also, stresses σ and strains ε on the mechanical side, as well as radial electric displacement D and electric field E on the electrostatic side, are arbitrarily combined according to [19] into two forms of coupled constitutive equations as follows:

$$\begin{Bmatrix}\sigma\\ D\end{Bmatrix} = \begin{bmatrix}C^{E} & -e\\ e^{T} & e^{\varepsilon}\end{bmatrix}\begin{Bmatrix}\varepsilon\\ E\end{Bmatrix}, \qquad \begin{Bmatrix}\varepsilon\\ D\end{Bmatrix} = \begin{bmatrix}S^{E} & d\\ d^{T} & \in^{\sigma}\end{bmatrix}\begin{Bmatrix}\sigma\\ E\end{Bmatrix} \tag{24}$$

Therefore, constants of the matrices *e* and *d* correspond to induced stress and strain, respectively *C*, *S* and $\in$ are compliance matrix, stiffness matrix and dielectric constants, respectively [15].

3.3 Circular plate theory

As presented in Fig. 1, the nanocomposite annular plate considered with inner and outer radius of a and b respectively and is subjected to axisymmetric thermo-mechanical and electrical loadings. To model the assembly of layers or laminae of materials with piezoelectric properties, it has been suggested by [19] to extend the classical lamination theory for conventional laminates [20, 21]. According to CLPT, normal and shear strains transverse to the laminate are assumed to be negligibly small. The stresses and radial electric displacement of the layer are hence determined as follows:

$$\begin{Bmatrix}\sigma_r\\ \sigma_\theta\\ \tau_{r\theta}\\ D_1\end{Bmatrix} = \bar{C}\begin{Bmatrix}\varepsilon_r\\ \varepsilon_\theta\\ \gamma_{r\theta}\\ \bar{E}_1\end{Bmatrix} \tag{25}$$

where σ_r and σ_θ are normal stresses in r and θ directions, respectively. $\tau_{r\theta}$ is the shear stress in $r\theta$ plane. D_1 is the electrical displacement in radial direction, as indicated in Fig. 1. Defining N and Mas in-plane and out-of plane resultants, respectively, and using the appropriate subscript, for the overall structure, we have [19]:

$$N = \begin{Bmatrix} N_r \\ N_\theta \\ N_{r\theta} \\ G_1 \end{Bmatrix} = \int_{-h/2}^{h/2} \begin{Bmatrix} \sigma_r \\ \sigma_\theta \\ \tau_{r\theta} \\ D_1 \end{Bmatrix} \mathrm{dz}, \tag{26a}$$

$$M = \begin{Bmatrix} M_r \\ M_\theta \\ M_{r\theta} \\ H_1 \end{Bmatrix} = \int_{-h/2}^{h/2} \begin{Bmatrix} \sigma_r \\ \sigma_\theta \\ \tau_{r\theta} \\ D_1 \end{Bmatrix} z\,\mathrm{dz} \tag{26b}$$

3.4 Strain displacement relations

In order to calculate the mid-surface strain and curvatures, using classical plate theory assumptions, the displacement components of an arbitrary point anywhere are written as [13]:

$$\begin{aligned} u_r(r,\theta,z) &= u_{0r}(r,\theta) - z\frac{\partial w(r,\theta)}{\partial r} \\ u_\theta(r,\theta,z) &= u_{0\theta}(r,\theta) - \frac{z}{r}\frac{\partial w(r,\theta)}{\partial \theta} \\ w(r,\theta,z) &= w_0(r,\theta) \end{aligned} \tag{27}$$

where u_{0r}, $u_{0\theta}$ and w_0 are the displacement of mid-plane in $r-$and $\theta-$directions respectively, which are assumed to be zero because there is no coupling between the in-plane and the out-of-plane displacements. $w(r,\theta,z)$ denotes the displacement in $z-$direction or lateral deflection of the composite plate.

4 BUCKLING ANALYSIS

4.1 Total potential energy

Total potential energy for an elastic body is expressed as [22]:

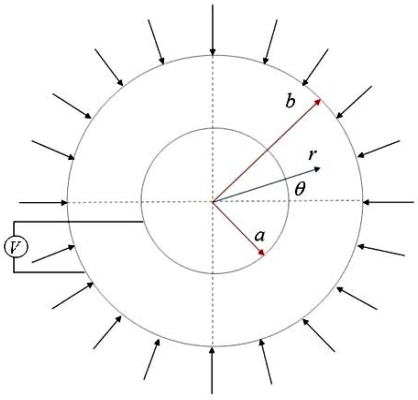

Fig. 1
Schematic of annular circular plate.

$$V = U - \int_{s_r} T_i u_i \mathrm{d}S - \int_V F_i u_i \mathrm{d}V \tag{28}$$

where, the first term on right hand side is electrostatic energy. The second and third terms represent the work done by the surface tractions and the body forces, respectively.

The electroelastic energy density determined generally as [19]:

$$u_0 = u_0^{md} - u_0^{ep} \tag{29}$$

where u_0^{md} is the strain energy density and u_0^{ep} is the electrical potential energy density [20]. Integrating over the entire structure gives the electroelastic energy, i.e.:

$$U = \frac{1}{2}\int_\Lambda u_0 \,\mathrm{d}V = \frac{1}{2}\left[\int_\Lambda \varepsilon^T \sigma \,\mathrm{d}V - \int_\Lambda E^T D \,\mathrm{d}V\right] = \frac{1}{2}\int_\Lambda \begin{Bmatrix}\varepsilon^T & \bar{E}^T\end{Bmatrix}\begin{Bmatrix}\sigma \\ D\end{Bmatrix}\mathrm{d}V, \qquad \bar{E} = -E \tag{30}$$

Substituting Eq. (24) into Eq. (30), we have

$$U = \frac{1}{2}\int_\Lambda \begin{Bmatrix}\varepsilon^T & \bar{E}^T\end{Bmatrix}\underbrace{\begin{bmatrix}C^E & e \\ e^T & -\in^\varepsilon\end{bmatrix}}_{\bar{\mathbf{C}}}\begin{Bmatrix}\varepsilon \\ \bar{E}\end{Bmatrix}\mathrm{d}V, \qquad \bar{E} = -E = -\frac{V}{d}, \quad \bar{\mathbf{C}} = \bar{\mathbf{C}}^T \tag{31}$$

V and *d* denote voltage difference and the difference between *a* and *b*, respectively (see Fig. 1). Assuming uniform electrical fields, Eq. (30) becomes

$$U = \frac{1}{2}\int_\Lambda \begin{Bmatrix}\varepsilon_r & \varepsilon_\theta & \bar{E}_1\end{Bmatrix}\begin{bmatrix}C_{11} & C_{12} & e_{11} \\ C_{12} & C_{12} & e_{12} \\ e_{11} & e_{12} & -\in_{11}\end{bmatrix}\begin{bmatrix}\varepsilon_r \\ \varepsilon_\theta \\ \bar{E}_1\end{bmatrix}\mathrm{d}V \tag{32}$$

where C_{ij}, e_{ij} and $\in_{ij}$ are the on-axis elastic coefficients of composites in polar coordinate system, piezoelectric constants and dielectric constants, respectively.

Strain-displacement relations in polar coordination are [22]:

$$\varepsilon_r = \frac{\partial u_{0r}}{\partial r} - z\frac{\partial^2 w}{\partial r^2} \tag{33a}$$

$$\varepsilon_\theta = \frac{1}{r}\frac{\partial u_{0\theta}}{\partial \theta} + \frac{u_{0r}}{r} - \frac{z}{r^2}\frac{\partial^2 w}{\partial \theta^2} - \frac{z}{r}\frac{\partial w}{\partial r} \tag{33b}$$

$$\gamma_{r\theta} = \frac{1}{2}\left(\frac{1}{r}\frac{\partial u_{0r}}{\partial \theta} - \frac{\partial u_{0\theta}}{\partial r} - \frac{u_{0\theta}}{r}\right) - \frac{2z}{r}\frac{\partial^2 w}{\partial r \partial \theta} + \frac{2z}{r^2}\frac{\partial w}{\partial \theta} \tag{33c}$$

Radial and circumferential mid-plane displacements in *r* and θ directions are neglected. Also, stress and strain in thickness direction are ignored. Therefore, Eqs. (33a-33c) are simplified as follows:

$$\varepsilon_r = -z\frac{\partial^2 w}{\partial r^2} \tag{34a}$$

$$\varepsilon_\theta = -\frac{z}{r}\frac{\partial w}{\partial r} \tag{34b}$$

$$\gamma_{r\theta} = 0 \tag{34c}$$

Applying matrix multiplication on Eq. (32) gives:

$$U = \frac{1}{2}\int (C_{11}\varepsilon_r^2 + 2C_{12}\varepsilon_r\varepsilon_\theta + 2\bar{E}_1 e_{12}\varepsilon_\theta + C_{22}\varepsilon_\theta^2 + 2\bar{E}_1 e_{11}\varepsilon_r - \in_{11}\bar{E}_1^2)\mathrm{d}V \tag{35}$$

Substituting Eqs. (34a-34c) into Eq. (35) gives the electrostatic energy as:

$$\begin{aligned} U = \frac{1}{2}\int_0^{2\pi}\int_a^b\int_{-h/2}^{h/2}\Bigg[& C_{11}\left[-z\frac{\partial^2 w}{\partial r^2} - \alpha_r\Delta T\right]^2 + 2C_{12}\left[-z\frac{\partial^2 w}{\partial r^2} - \alpha_r\Delta T\right]\left[-\frac{z}{r}\frac{\partial w}{\partial r} - \alpha_\theta\Delta T\right] \\ & + 2\bar{E}_1 e_{12}\left[-\frac{z}{r}\frac{\partial w}{r} - \alpha_\theta\Delta T\right] + \bar{C}_{22}\left[-\frac{z}{r}\frac{\partial w}{\partial r} - \alpha_\theta\Delta T\right]^2 + 2\bar{E}_1 e_{11}\left[-z\frac{\partial^2 w}{\partial r^2} - \alpha_r\Delta T\right] - \in_{11}\bar{E}_1^2\Bigg] r\,\mathrm{d}z\,\mathrm{d}r\,\mathrm{d}\theta \end{aligned} \tag{36}$$

Work done by traction forces are expressed as [20]:

$$\int_{Sr} T_i u_i \mathrm{d}S = \int_0^{2\pi}\int_a^b N_r\left[\frac{\partial u_0}{\partial r} + \frac{1}{2}\left(\frac{\partial w}{\partial r}\right)^2\right] r\,\mathrm{d}r\,\mathrm{d}\theta \tag{37}$$

where N_r is applied axial force on two edges of cylinder which is defined as:

$$N_r = N_r^{mech} + N_r^T + N_r^E, \qquad N_{ij}^T = \int_{-\frac{h}{2}}^{\frac{h}{2}} (\mathrm{C_{ij}})\alpha_{ij}\,\Delta T\,\mathrm{d}z, \qquad N_{ij}^E = \int_{-\frac{h}{2}}^{\frac{h}{2}} (\mathrm{e_{ij}})\bar{E}_{ij}\mathrm{d}z, \tag{38}$$

where N_r^{mech}, N_r^T and N_r^E are mechanical, thermal and electrical forces, respectively. Using Eq. (28), the total potential energy of the composite shell is obtained as:

$$\begin{aligned} V = \frac{1}{2}\int_0^{2\pi}\int_a^b\int_{-\frac{h}{2}}^{\frac{h}{2}}\Bigg[& C_{11}\left[\left(z\frac{\partial^2 w}{\partial r^2}\right)^2 + \left(\alpha_r\Delta T\right)^2 + 2z\frac{\partial^2 w}{\partial r^2}\alpha_r\Delta T\right] \\ & + 2C_{12}\left[\frac{z^2}{r}\frac{\partial^2 w}{\partial r^2}\frac{\partial w}{\partial r} + z\alpha_\theta\Delta T\frac{\partial^2 w}{\partial r^2} + \frac{z\alpha_r}{r}\Delta T\frac{\partial w}{\partial r} + \alpha_r\alpha_\theta\Delta T^2\right] + 2\bar{E}_1 e_{12}\left[-\frac{z}{r}\frac{\partial w}{\partial r} - \alpha_\theta\Delta T\right] \\ & + C_{22}\left[\left(\frac{z}{r}\frac{\partial w}{\partial r}\right)^2 + \left(\alpha_\theta\Delta T\right)^2 + \frac{2z}{r}\frac{\partial w}{\partial r}\alpha_r\Delta T\right] \\ & + 2\bar{E}_1 e_{11}\left[-z\frac{\partial^2 w}{\partial r^2} - \alpha_r\Delta T\right] - \in_{11}\bar{E}_1^2\Bigg] r\,\mathrm{d}z\,\mathrm{d}r\,\mathrm{d}\theta \\ & - \int_0^{2\pi}\int_a^b\left[N_r + \int_{-\frac{h}{2}}^{\frac{h}{2}}\left[(C_{11}\alpha_r + C_{12}\alpha_\theta)\Delta T + e_{11}\bar{E}_1\right]dz\right]\left[\frac{1}{2}\left(\frac{\partial w}{\partial r}\right)^2\right] r\,\mathrm{d}r\,\mathrm{d}\theta \end{aligned} \tag{39}$$

where *a*,*b* and *h* are inner radius, outer radius and thickness of the circular plate, respectively.

$$V=\frac{1}{2}\int_0^{2\pi}\int_a^b\left[C_{11}\left[\frac{h^3}{12}\left(\frac{\partial^2 w}{\partial r^2}\right)^2+h(\alpha_r\Delta T)^2\right]+2C_{12}\left[\frac{h^3}{12}\frac{1}{r}\frac{\partial^2 w}{\partial r^2}\frac{\partial w}{\partial r}+h\alpha_r\alpha_\theta\Delta T^2\right]\right.$$
$$-2\bar{E}_1 e_{12}h\alpha_\theta\Delta T+C_{22}\left[\frac{h^3}{12}\frac{1}{r^2}\left(\frac{\partial w}{\partial r}\right)^2+h(\alpha_\theta\Delta T)^2\right]-2\bar{E}_1 e_{11}h\alpha_r\Delta T \quad (40)$$
$$\left.-h\in_{11}\bar{E}_1^2-\left[N_r+\left(C_{11}\alpha_r+C_{12}\alpha_\theta\right)h\Delta T+e_{11}\bar{E}_1 h\right]\left(\frac{\partial w}{\partial r}\right)^2\right]r\,\mathrm{d}r\,\mathrm{d}\theta$$

4.2 Boundary conditions

In this article, two boundary conditions for annular composite plate are considered; Case 1. referring to an annular plate simply supported on two edges and Case 2 .referring to an annular plate with edges being clamped on both sides. These boundary conditions are described mathematically as follows:
Case1) Simple support

$$w=0; \quad \text{at} \quad r=a \ \text{and} \ b,$$
$$\frac{\partial^2 w}{\partial r^2}=0; \quad \text{at} \quad r=a \ \text{and} \ b. \quad (41)$$

For satisfying these conditions, the following function is assumed for the lateral displacement [13]

$$w=\sum_{P=1}^{\infty}A_p\sin\frac{p\pi(b-r)}{b-a} \quad (42)$$

Case2) Clamped support

$$w=0; \quad \text{at} \quad r=a \ \text{and} \ b,$$
$$\frac{\partial w}{\partial r}=0; \quad \text{at} \quad r=a \ \text{and} \ b. \quad (43)$$

Similarly, the following function is assumed to describe the lateral displacement [13]

$$w=\sum_{p=1}^{\infty}A_p\left(1-\cos\frac{2p\pi(b-r)}{b-a}\right) \quad (44)$$

4.3 Minimum total potential energy method

According to the definition of minimum potential energy, of all the displacements satisfying compatibility and the prescribed boundary conditions, those that satisfy the equilibrium equations make the potential energy a minimum [20]. Mathematically, this happens when $\delta V=0$.

Substituting the lateral displacement in total potential energy and applying minimum potential energy principle, the axial buckling force of composite shells may be expressed as below for the two cases of boundary conditions stated above:

Case 1:

$$N_r = \frac{C_{11}\frac{h^3}{12}\left(\frac{P\pi}{b-a}\right)^2\left(\frac{b^2-a^2}{4}\right)+C_{22}\frac{h^3}{12}\int_a^b \frac{1}{r}\cos^2\frac{P\pi(b-r)}{(b-a)}\mathrm{d}r}{\frac{b^2-a^2}{4}} - (C_{11}\alpha_r + C_{12}\alpha_\theta)h\Delta T - \frac{e_{11}h}{b-a}V \tag{45}$$

Case 2:

$$N_r = \frac{C_{11}\frac{h^3}{12}\left(\frac{2P\pi}{b-a}\right)^2\left(\frac{b^2-a^2}{4}\right)+C_{22}\frac{h^3}{12}\int_a^b \frac{1}{r}\sin^2\frac{2P\pi(b-r)}{(b-a)}\mathrm{d}r}{\frac{b^2-a^2}{4}} - (C_{11}\alpha_r + C_{12}\alpha_\theta)h\Delta T - \frac{e_{11}h}{b-a}V \tag{46}$$

5 NUMERICAL RESULTS AND DISCUTION

In this section, numerical results on the effects of thermal and electrical loads on radially compressed buckling of the piezoelectric annular plate are investigated. Using modeling procedure described above and Eqs. (45-46), the numerical results of the critical buckling load are demonstrated in Figs. 2 to 6. The nanotube considered as fiber in this study is BNNT, with the zigzag structure, has Young's modulus E=1.8 TPa, the axial and circumferential thermal expansion coefficients ($\alpha_r = 1.2e-6$ and $\alpha_\theta = 0.6e-6$) and piezoelectric constant $e_{11} = 0.95\,\mathrm{C/m^2}$ [23].

The properties of PVDF considered as matrix are [21]: $C_{11} = 238.24\,\mathrm{GPa}$, $C_{22} = 23.6\,\mathrm{GPa}$, $C_{66} = 6.43\,\mathrm{GPa}$, $C_{12} = 3.98\,\mathrm{GPa}$, $e_{11} = -0.13\,\mathrm{C/m^2}$ and $\alpha_r = \alpha_\theta = 7.1e-5\,(1/^\circ\mathrm{C})$. The geometrical properties of annular plate are: $a = 4e-5\,\mathrm{m}$, $b = 1e-4\,\mathrm{m}$, $h = 1e-6\,m$ Temperature change and applied voltage are $20^\circ\mathrm{C}$ and 4000 V, respectively.

Radial buckling load (N_r) is plotted as a function of inner-to-outer radius ratio (a/b) under mechanical load for the two cases of boundary conditions and different BNNT volume fraction (C_r) in Figs. 2a and 2b. Increasing a/b leads to an increase in buckling load. N_r rises with increasing the BNNT volume fraction. So that the highest radial buckling load occurs in $C_r = 0.2$. This implies that the stiffness of structure increases with the increase in BNNT volume fraction. Moreover, by improving elastic properties of nanocomposite, buckling occurred in smaller a/b in constant load. As far as the simple and clamped boundary conditions are concerned, generally in the former, N_r is smaller in magnitude, showing the significance of the boundary conditions on the two edges under buckling load of the annular plate.

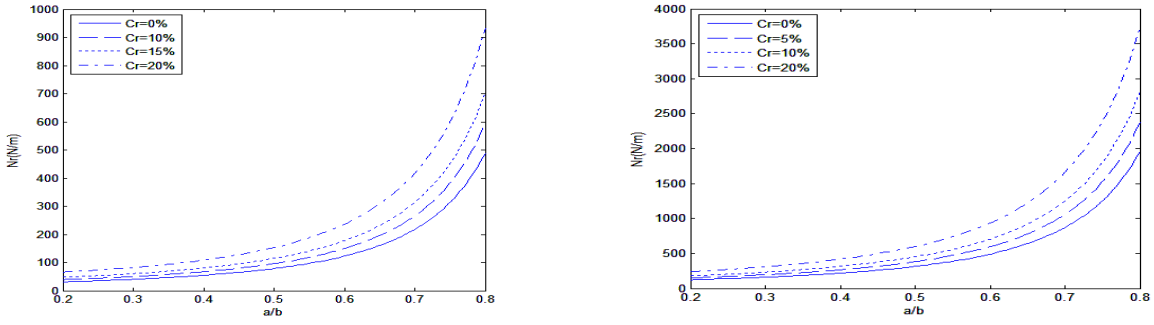

(a) (b)

Fig. 2
Axisymmetric buckling load, versus inner-to-outer radius ratio (a/b) for (a) simple support, and (b) clamped support (BNNT volume fraction=0, 5, 10, 20%)

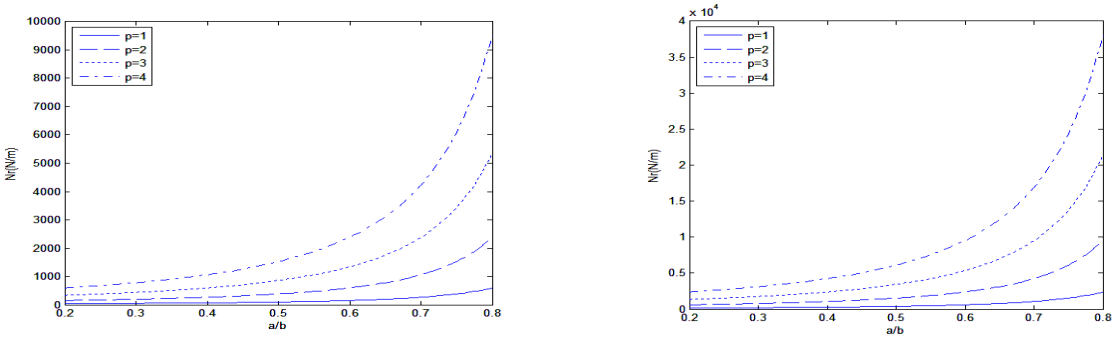

(a) (b)

Fig. 3
Axisymmetric buckling load, versus inner-to-outer radius ratio (a/b) for (a) simple support, and (b) clamped support (mode number=1,2,3,4, C_r=5%).

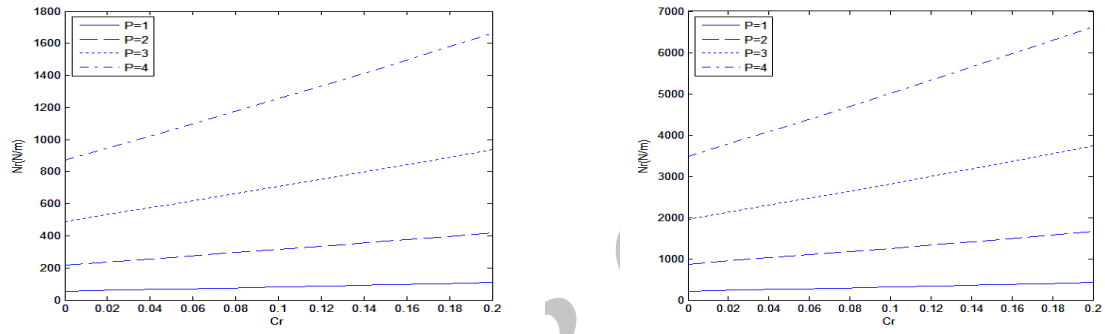

(a) (b)

Fig. 4
Axisymmetric buckling load, versus CNT volume fraction (C_r) for (a) simple support, and (b) clamped support (mode number=1, 2, 3, 4, a/b=0.4).

In Fig. 3a and 3b, radial buckling load versus the variation of a/b are plotted for four first mode numbers (p=1-4) and two boundary conditions to illustrate the influence of a/b on higher buckling modes for both simply and clamped supported edge. It can be seen that N_r tends to increase with increase in a/b with the slope being increased continuously for higher p. It means the effect of a/b is higher for higher p. The effect of BNNT volume fraction on buckling load is illustrated for two boundary conditions considered in Figs. 4a and 4b N_r increases with increasing C_r for a constant p. It is clear that the difference between curves increases with increase C_r.

Figs. 5a and 5b show the combined and isolated effects of thermal, electrical as well as mechanical fields on the radial buckling load of annular plate. Uniform temperature change and applied voltage are $\Delta T = \pm 20\,\mathrm{K}$ and $V = \pm 4000\,\mathrm{V}$, respectively. Applying direct voltage increases N_r due to polarization created in the piezoelectric in the radial direction leading to its contraction. This makes piezoelectric more compact and stable in loading direction. Similar results are achieved when annular plate temperature is reduced. Thermal strains producing in radial direction affect the radial buckling load and positive temperature change causes reducing N_r. A small change in the temperature filed will bring about large changes in the magnitude of radial buckling load. As can be seen, the effect of thermal filed is much more than electric field in magnitude. Figs. 6a and 6b show the effect of BNNT volume fraction on the radial buckling load in presence of the combined and isolated thermal, electrical and mechanical fields. Similar to Figs.4 increasing BNNT volume fraction increases buckling load. The effect of thermal field decreases in higher C_r due to the fact that thermal expansion coefficients of BNNT are much smaller than PVDF. According to different sign of piezoelectric constants of BNNT and PVDF, by increasing C_r, they neutralize the electrical effect of each other.

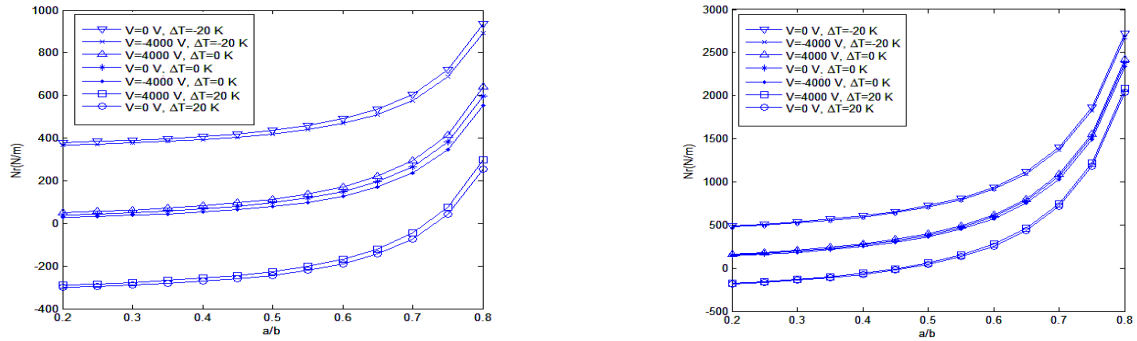

(a) (b)

Fig. 5
Axisymmetric buckling load, versus inner-to-outer radius ratio (C_r) for (a) simple support, and (b) clamped support (different thermal and electrical fields, $C_r = 5\%$, $p = 1$).

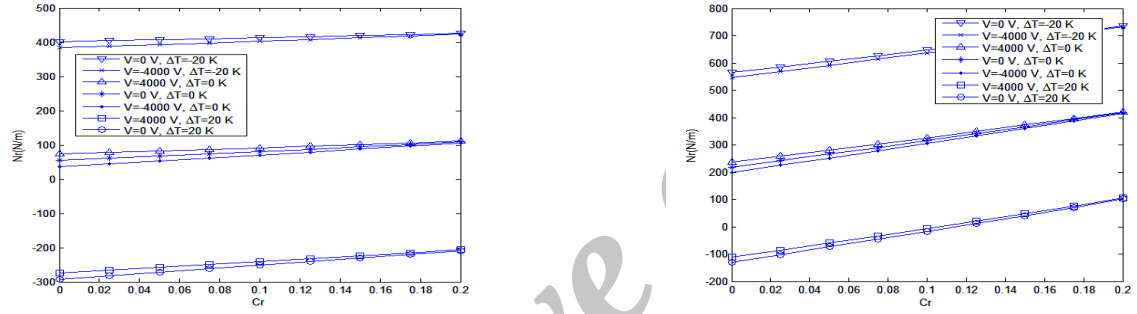

(a) (b)

Fig. 6
Axisymmetric buckling load, versus BNNT volume fraction (C_r) for (a) simple support, and (b) clamped support (different thermal and electrical fields, a/b=0.4, p=1).

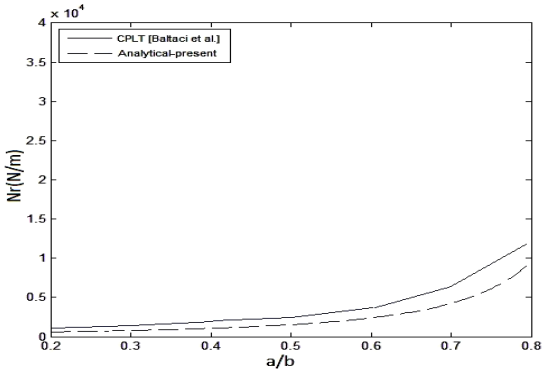

Fig. 7
Axisymmetric buckling load, versus BNNT volume fraction (C_r) for clamped boundary condition (Comparison of present work with CLPT result from [16], a/b=0.4, p=1).

According to the review of previsions literatures, no similar work has been done about the buckling of piezoelectric nanocomposite plates considering multi physical fields such as thermal, mechanical and electric loads. Although there is not any same investigation, the numerical results and the figures trend of this article are in accordance with similar studies on buckling load of annular plates [16, 17]. Fig. 7 illustrates a partially comparison

between present study and work done by Baltaci et al. [16] to validate the accuracy of the present work. In the comparison, the effect of mechanical loads is only considered. We compared the results of energy method with results of CLPT. The results of two mentioned methods have good agreement for case of clamped boundary condition and small values of *a*/*b*.

6 CONCLUSIONS

In this study, minimum potential energy approach is used to evaluate the axisymmetric buckling load behavior in a piezoelectric polymeric annular plate reinforced with DWBNNT subjected to combined electro-thermo-mechanical loadings. Classical boundary conditions of simple and clamped supports are considered for this. Coupling between electrical and mechanical fields are considered according to a RVE-based micromechanical model. The results indicate that increasing inner-to-outer radius ratio yields to an increase in buckling load. The buckling load rises with increasing the BNNT volume fraction and the stiffness of composite structure increases. Buckling load in simply supported condition is smaller than clamped one. Moreover, buckling load tends to increase with inner-to-outer radius ratio and the influence of that is higher for higher mode number. It is shown that buckling resistance of composite annular plate varies by applying thermal and electrical loads. Employing direct voltage or decreasing the temperature increases buckling load. The results show that adding BNNTs to PVDF has a significant influence on the electro-thermo- mechanical behavior of nanocomposite and hence should be considered in optimum design. The buckling instability of nanocomposite structure can be controlled by employing thermal and electrical loads along with external forces. Also, at normal working conditions, the influence of thermal and mechanical fields are much higher than the electric one on the buckling load; hence, this smart structure is best suited for applications as sensors than actuators.

ACKNOWLEDGMENTS

The author would like to thank the reviewers for their reports to improve the clarity of this article. The authors are grateful to University of Kashan for supporting this work by Grant No. 65475/29. They would also like to thank the Iranian Nanotechnology Development Committee for their financial support.

REFERENCES

[1] Rubio A., Corkill J. L., Cohen M. L., 1994, Theory of graphitic boron nitride nanotubes, *Physical Review B* **49**: 5081-5084.

[2] Blasé X., Rubio A., Louie S. G., Cohen M. L., 1994, Stability and band gap constancy of boron nitride nanotubes, *Europhysics Letters* **28**: 335-340.

[3] Chen Y., Zou J., Campbell S.J., Caer G.L., 2004, Boron nitride nanotubes: Pronounced resistance to oxidation, *Applied Physics Letters* **84**: 2430-2432.

[4] Sai N., Mele E. J., 2003, Microscopic theory for nanotube piezoelectricity, *Physical Review B* **68**: 241405.

[5] Bansal N.P., Hurst J.B., Choi S.R., 2006, Boron nitride nanotube-reinforced glass composites, *Journal of the American Ceramic Society* **89**: 388-390.

[6] Munch W.V., Thiemann U. 1991, Pyroelectric detector array with PVDF on silicon integrated circuit, *Sensors and Actuators A: Physical* **25**: 167-172.

[7] Xing S., 2002, Novel piezoelectric and pyroelectric materials: PVDF copolymer-carbon nanotubes composites, Master's Thesis, Department of Material Science and Engineering, Clemson University.

[8] Crawley E.F., 1994, Intelligent structures for aerospace: a technology overview and assessment, *AIAA Journal* **32**: 1689-99.

[9] Niezrecki C., Brei D., Balakrishnan S., Moskalik A., 2001, Piezoelectric Actuation: State of the Art, *The Shock and Vibration Digest* **33**: 269-280.

[10] Wilkie W.K., Bryant R.G., High J.W., Fox R.L., Hellbaum R.F., Jalink A., Little B.D., Mirick P.H., 2000, Low-cost piezocomposite actuator for structural control applications, in: *Proceedings of Seventh SPIE International Symposium on Smart Structures and Materials*, Newport Beach, CA, March 5-9.

[11] Najafizadeh M.M., Heydari, H.R., 2008, An exact solution for buckling of functionally graded circular plates based on higher order shear deformation plate theory under uniform radial compression, *International Journal of Mechanical Sciences* **50**: 603-612.

[12] Ghorbanpour Arani A., Maghamikia Sh., Mohammadimehr M., Arefmanesh A., 2011, Buckling analysis of laminated composite rectangular plates reinforced by SWCNTs using analytical and finite element methods, *Journal of Mechanical Science and Technology* **25**(3): 809-820.
[13] Jam J. E., Kia S. M., Pour A. G., Emdadi M., 2011, Elastic buckling of circular annular plate reinforced with carbon nanotubes, *Polymer Composites* **32**(6): 896-903.
[14] Vodenitcharova T., Zhang L.C., 2006, Bending and local buckling of a nanocomposite beam reinforced by a single-walled carbon nanotube, *International Journal of Solids and Structures* **43**: 3006-3024.
[15] Shen H.S., Zhang C.L., 2010, Thermal buckling and post buckling behavior of functionally graded carbon nanotube-reinforced composite plates, *Materials & Design* **3**: 3403-3411.
[16] Baltaci A., Sarikanat M., Yildiz H., 2007, Static stability of laminated composite circular plates with holes using shear deformation theory, *Finite Elements in Analysis and Design* **43**: 839-846.
[17] Seifi R., Khoda-yari N., Hosseini H., 2012, Study of critical buckling loads and modes of cross-ply laminated annular plates, *Composites Part B: Engineering* **43**: 422-430.
[18] Tan P., Tong L., 2001, Micro-electromechanics models for piezoelectric-fiber-reinforced composite materials, *Composites Science and Technology* **61**: 759-69.
[19] Brockmann T.H., 2009, *Theory of Adaptive Fiber Composites From Piezoelectric Material Behavior to Dynamics of Rotating Structures*. Springer.
[20] Jones R.M., 1975, *Mechanics of Composite Materials*, Scripta Book Company, Washington.
[21] Whitney J.M., 1987, *Structural Analysis of Laminated Anisotropic Plates*, Technomic Publishing Company, Lancaster.
[22] Vinson J.R., 2005, *Plate and Panel Structures of Isotropic, Composite and Piezoelectric Materials, Including Sandwich Construction*, Springer.
[23] Salehi-Khojin A., Jalili N., 2008, Buckling of boron nitride nanotube reinforced piezoelectric polymeric composites subject to combined electro-thermo-mechanical loadings, *Composites Science and Technology* **68**: 1489-1501.
357-372.